The high-speed rotorcraft unmanned aerial vehicle path planning based on the biogeography-based optimization algorithm

Jia Song[1] (iD), Mingfei Zhao[1] (iD), Erfu Yang[2] and Jiaming Lin[1]

Abstract

A three-dimensional path planning method based on the biogeography-based optimization algorithm is presented for high-speed rotorcraft unmanned aerial vehicle which has a maximum speed of 20 m/s. In this study, a novel exponential artificial potential field is used to prevent saturation, for its peculiarity of smoothness and boundness. Several parameters, which can make a large influence to the result of path planning, are picked out and used to improve the process of planning. Biogeography-based optimization algorithm is first used to optimize the parameters of artificial potential fields, for its best performance in stability and speed. The algorithm has good stability and fast operation speed, which can realize the global path planning of multi-rotor aircraft well, verified by the simulation results.

Keywords

High-speed rotorcraft, biogeography-based optimization, three-dimensional path planning, artificial potential field, unmanned aerial vehicles

Introduction

Recently, the unmanned aerial vehicles (UAVs) have developed rapidly, but there are many serious problems to solve in the field of UAV security control. The security control which is an important part of UAV control contains flight reliability, fault-tolerant control, autonomous obstacle avoidance, anti-jamming, and flight mission management.

The most needed, in the field, is the development of autonomous obstacle avoidance, because the most UAV flight accidents are caused by hitting obstacles. For example, when there is a need of UAV in rescues or in geological prospecting, the obstacles such as trees, rock even birds that UAV must past through may disturb the UAV flight even cause UAV crash. Another example, when UAV is used in transportation, how to elude high buildings is the most important thing that should be considered.

Figure 1 is the UAV of FLA (fast lightweight autonomy), which belongs to DARPA (Defense Advanced Research Projects Agency). Target of the project is to develop one UAV which can fly at the speed of 45 miles per hour (20 m/s) to avoid obstacles.

The high-speed obstacle avoidance aircraft which is mentioned later in this article is the same kind to FLA and named high-speed rotorcraft, which flies at the maximum speed of 20 m/s. Two problems need to be solved in the process of high-speed obstacle avoidance.

[1]School of Astronautics, Beihang University, Beijing, China
[2]Space Mechatronic Systems Technology Laboratory, Strathclyde Space Institute, University of Strathclyde, Glasgow, UK

Corresponding author:
Mingfei Zhao, School of Astronautics, Beihang University, Beijing 100191, China.
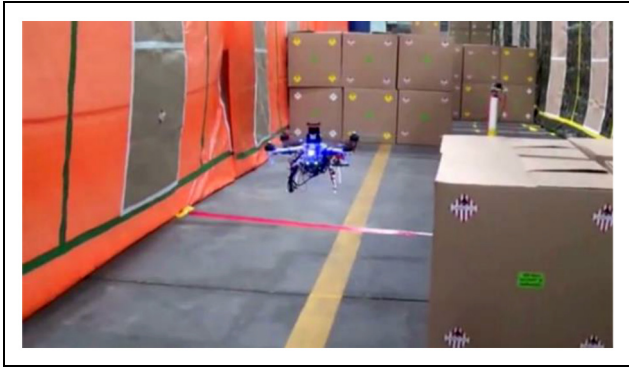Email: zmf1002@buaa.edu.cn

Figure 1. The UAV of FLA.

The first problem is flight control. When the four-rotor aircraft voyage with high speed, the attitude angle is very large and the control system is non-linear, the method of iterative learning is used to optimize the control volume to achieve high-precision maneuver in Lupashin and D'Andrea,[1] the optimal control and iterative learning method has obtained the same good control effect in Ritz et al.,[2] Mellinger et al.[3] use the method of iterative learning, and proportional–integral–derivative (PID) as the underlying control to obtain the high maneuvering motion of the four-rotor craft through the narrow hole.

The second problem is path planning. How to project a path that is feasible and short when the four-rotor aircraft voyage with high speed is discussed extensively. The problem is mainly discussed in this article. Some studies are made in path planning. A three-dimensional path planning method based on autonomous learning frame is proposed in Yang et al.,[4] the trajectory planning and simulation based on quadrotors are studied by Bouktir et al.[5] A star algorithm is used to deal with path planning of a mobile robot based on a grid map in Duchoň et al.[6] Dijkstra algorithm is used in the robot path planning.[7] A Floyd–Dijkstra hybrid application for path planning is presented for mobile robot transportation in life science laboratories.[8] An interpolation-based planning and replanning algorithm for generating low-cost paths through uniform and nonuniform resolution grids is presented by Ferguson and Stentz.[9] A genetic algorithm (GA)-based path planning software for mobile robot systems focusing on energy consumption is presented in Gemeinder and Gerke.[10] A multiobjective particle swarm optimization (PSO)-based algorithm is presented for robot motion planning with respect to two objectives, the shortest and smoothest path criteria in Masehian and Sedighizadeh.[11] Khatib[12] presents a unique real-time obstacle avoidance approach for manipulators and mobile robots based on the artificial potential field concept. Perez-Carabaza et al.[13] apply ant colony optimization (ACO) with novel heuristic function and encoding method on

UAVs minimum time search problem. Yao et al.[14] develop an optimal path planning method with Gaussian high value subregion extractor for coverage search problem. This method is working in 2D space, but the geographical constraints are considered. Yin et al.[15] propose a multiobjective path planning framework for low altitude urban environment. Oral and Polat[16] present a multiobjective D* algorithm which is built upon well-known D* algorithm for path planning problem under multiple objectives.

Artificial potential field, as one of the path planning method, has some advantages. The algorithm is simple and fast, which make it has great real-time performance. The path planned by this method is smooth. But the method of artificial potential field has its defects, such as the problem of local minima and unreachable destination.[17] For the past few years, research scholar has put forward many ways to perfect the method mentioned above. One method, that by connecting obstacles of the local minimum field to help aircraft walk out the boring field, is mentioned in Shi et al.[18] New repulsive potential functions are presented by taking the relative distance between the robot and the goal into consideration, which ensures that the goal position is the global minimum of the total potential in Ge and Cui.[19] Using potential field intensity but not force function in path planning, adding a modulus in repulsion field function and introducing velocity information to potential field function are all viable. Based on the modified model of artificial potential field, counting algebraic sum of all kinds of potential field intensity, then using genetic trust domain algorithm to get a minimum value of the sum in one cycle, all these minimum values constitute the best path.[20] Perfecting the method of artificial potential field by introducing velocities even accelerations of the aircraft relative to obstacles, and by judging avoiding action beforehand is mentioned in Wang et al.[21] Adding an additional force relying on obstacles when attraction and repulsion are collinear is mentioned in Zhang et al.[22] A best path is given in Kuang and Wang[23] based on GA. And in Liu,[24] a method of perfecting repulsion field function is presented. The above-mentioned studies have mainly focused on the two-dimensional path planning. However, there are few works on the three-dimensional path planning.

In this article, a modified artificial potential field is recommended to solve the path planning problem on the three-dimensional space. An exponential potential field force is used to replace traditional potential field force; the advantages of it contain two parts. Its force curve is bounded so that the force will never increase without limit. And the force curve is smooth which offer a better possibility of path planning.

There are many parameters that need to be adjusted when using artificial potential field to plan a route. In

this article, BBO (biogeography-based optimization) is cited to optimize these parameters. BBO was put forward in Ergezer et al.[25] first by Simon in 2008, and the algorithm was used for studying population generation, migration, and extinction patterns. Nowadays, BBO is widely used for optimizing parameters. Bhattacharya and Chattopadhyay[26] use BBO algorithm to solve the economic load dispatch problems of thermal plants. The result shows that BBO is able to find quality solution and has a better performance than other methods in case of complex type cost function. In hydraulic system, the result of control seems to be better when its PID parameters are optimized by BBO.[27] In tomato planting scheme, a hybrid BBO is used and a better result is obtained.[28] In Feng et al.,[29] a self-adapting BBO is expounded and used for global parameter optimization. One method called HBBO (hybrid biogeography-based optimization) is discussed in Mi et al.[30] Zheng et al.[31] modify the original BBO by introducing local topologies of habitats to rebalance the exploitation and the exploration of BBO. The new method called localized biogeography-based optimization (LBBO) shows better performance in various scenarios. But only in the simplest functions, original BBO is significantly better than LBBO. And based on previous research, Zheng et al.[32] improved LBBO using ecogeographic knowledge to establish the topology of habitat. However, BBO with single migration model is very difficult to obtain satisfactory solutions in different situations. Ma et al. present a BBO with an ensemble of migration model (BBO-EMM). The simulation result shows that BBO-EMM has better performance than BBO with single model.[33] Furthermore, Wang et al.[34] present a hyper-heuristic framework consist of different heuristic algorithms which could adaptively work together.

The structure of the present work is as follows. Section "Path planning model of high-speed rotorcraft" introduces the definitions of high-speed rotorcraft path planning. Section "The high-speed rotorcraft path planning based on the BBO algorithm" develops an optimization algorithm based on BBO, which is used for optimizing parameters of modified artificial potential field so that a better route can be founded. Section "Mathematical simulation" presents and discusses the mathematical simulation of two typical working conditions. Finally, the conclusions are drawn in section "Conclusion."

Path planning model of high-speed rotorcraft

High-speed rotorcraft model

The model of rotorcraft and the coordinate system are the same like Mahony's.[35] For the movement, the North-East-Down (NED) coordinates $(\vec{x}_e, \vec{y}_e, \vec{z}_e)$ and
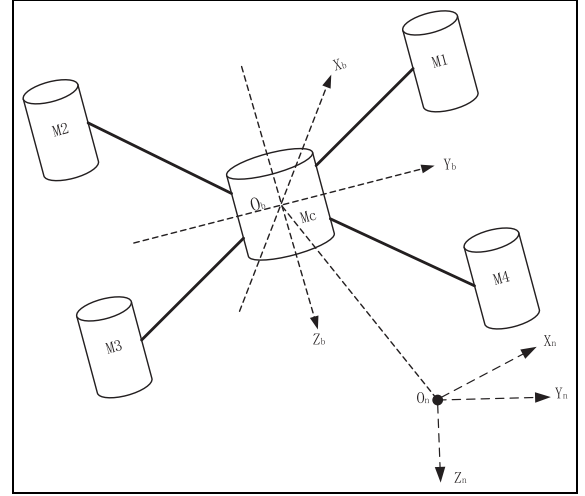

Figure 2. Body coordinate system and NED coordinate system.

the body coordinates $(\vec{x}_b, \vec{y}_b, \vec{z}_b)$ are involved. In this body coordinate, the linear velocity is written as $V_b = (u, v, w)^T$ (m/s), the angular velocity is written as $\omega = (p, q, r)^T$ (rad/s), the force is written as $F = (F_x, F_y, F_z)^T$ (N), and the torque is written as $\Gamma = (\Gamma_\varphi, \Gamma_\theta, \Gamma_\psi)^T$ (N m). The axis definition is described in Figure 2.

Motion model of high-speed rotorcrafts in the NED coordinate system is given as

$$\begin{cases} \dot{P}_n = R_{n/b} \cdot V_b \\ \dot{\Theta} = S^{-1} \cdot \omega \end{cases} \tag{1}$$

where $R_{n/b}$ means the coordinate transformation matrix from body coordinate to NED coordinate, P_n means displacement matrix of body coordinate system in NED coordinate system, ω means the angular velocity of vehicle in NED coordinate, and Θ means Euler angle matrix which describes the rotation of body coordinate system in NED coordinate system.

Dynamical model of high-speed rotorcrafts in the NED coordinate system is expressed as

Location model

$$\begin{cases} \dot{P}_n = v \\ m\dot{v} = mge_3 - R_{n/b}T \end{cases} \tag{2}$$

Posture model

$$\begin{cases} \dot{\Theta} = S^{-1} \cdot \omega \\ J\dot{\omega} = -\omega \times (J\omega) + \Gamma \end{cases} \tag{3}$$

where J is rotational inertia matrix of the aircraft, ω is angular velocity of the aircraft in body coordinate system, and $e_3 = [001]^T$ is unit vector of Z_n.

Sensor	Direction	
	$\theta(°)$	$\varphi(°)$
Sensor 1	0	0
Sensor 2	0	30
Sensor 3	0	−30
Sensor 4	0	60
Sensor 5	0	−60
Sensor 6	60	0
Sensor 7	−60	0
Sensor 8	60	30
Sensor 9	60	−30
Sensor 10	60	60
Sensor 11	60	−60
Sensor 12	−60	30
Sensor 13	−60	−30
Sensor 14	−60	60
Sensor 15	−60	−60

Figure 3. Repulsive force curve of high-speed rotorcraft.

In this article, in order to simplify calculated amount of path planning, the UAV is assumed to be able to track expect states. Besides, velocity of the vehicle is assumed to be less than 20 m/s. And acceleration is assumed to be less than 50 m/s².

There are 15 sensors used to detect the distance between vehicle and obstacles in 15 different directions. The orientations can be described in polar coordinate system in which θ is the angle between sensor direction and z-axis, φ is the angle between the projection of sensor direction on xOy surface and x-axis.

It is necessary to select the appropriate objective function. There are two main considerations in the process of path planning, that is, path length and time cost. There are some contradictions between these two requirements. The objective function is

$$f(s,t) = s + \beta * t \qquad (4)$$

where β is weight coefficient

$$\{0 < \beta < 1\}$$

s is path length and t is time cost. In this article, β is set as 16 according to the maximum velocity to make the path length factor and the time cost factor on the same scale.

Artificial attractive potential field of high-speed rotorcraft

Artificial attractive force gives aircraft a signal to make it fly to the target. The function of artificial attractive potential field is

$$U_{att} = \frac{1}{2} k_{att} (x - x_g)^2 \qquad (5)$$

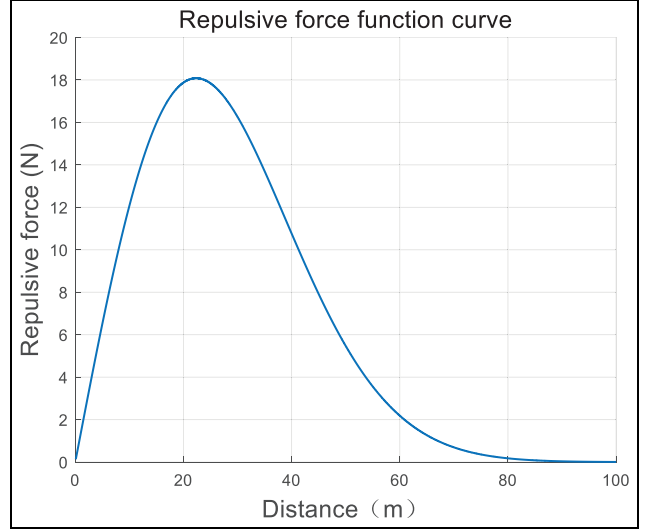where x is the position of vehicle and x_g is the position of goal. A scale factor of velocity is introduced in artificial attractive force in order to confirm system asymptotically stability, so the artificial attractive force is expressed as

$$F_{att} = -k_{att} p^* - k_{atv} \dot{x} \qquad (6)$$

where p^* denotes the vector indicating the position of the target relative to the aircraft, k_{att} is the coefficient of artificial attractive potential field, k_{atv} is a scale factor of velocity, and $\dot{x}$ is the velocity vector.

Artificial repulsion potential field of high-speed rotorcraft

Artificial repulsion force is used for controlling the aircraft stay away from the obstacle. The function of repulsion potential field is

$$U_{rep} = \sum_i k_{rep} e^{-l_{rep} \|p_i - x_0\|^2} \qquad (7)$$

Therefore, the repulsion force is

$$F_{rep} = \sum_i 2 k_{rep} l_{rep} (p_i - x_0) e^{-l_{rep} \|p_i - x_0\|^2} \qquad (8)$$

where p_i is the vector indicating the position of aircraft relative to the obstacle detected by ith sensor, k_{rep} and l_{rep} are positive and transformable coefficients, and x_0 is the constant vector. When $x_0 = 0$, the curve of repulsion force is given as shown in Figure 3.

From Figure 3, it can be seen that the force is bounded when the aircraft is very close to the obstacle. This characteristic of the force can prevent high-speed rotorcraft control saturation of attitude angles and reduce oscillation of the angles. In addition, the curve is smooth so that optimizing of the route could be easier.
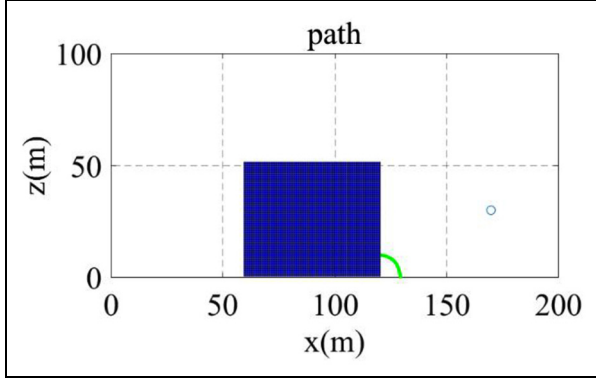
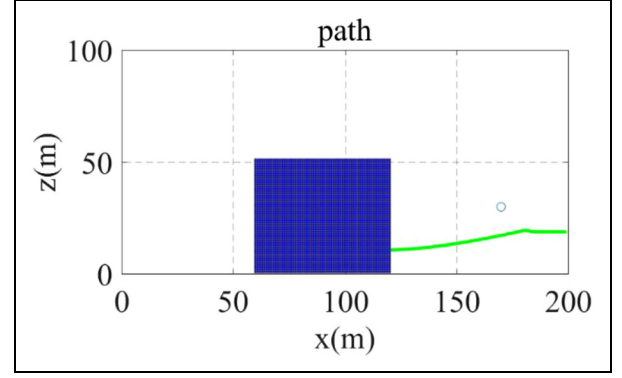**Figure 4.** Flight path of contrastive example.

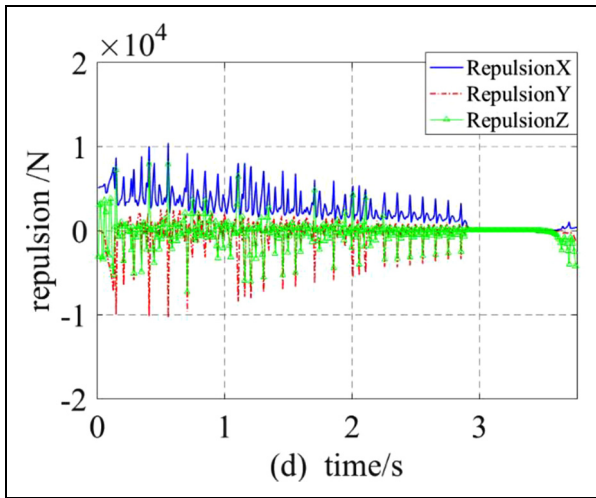**Figure 6.** Flight path with exponential repulsion function.

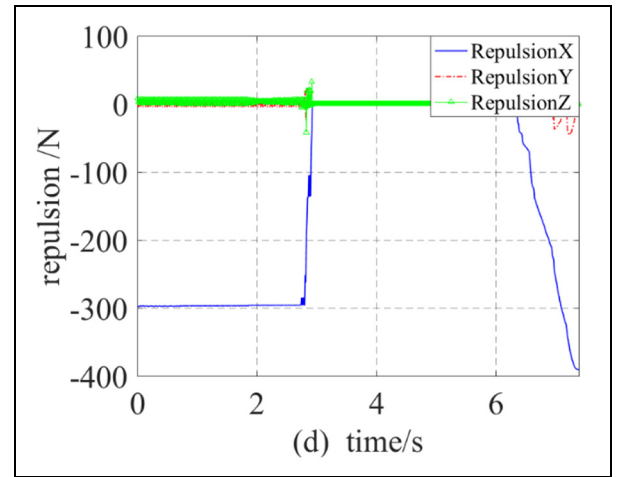**Figure 5.** Artificial repulsion of contrastive example.

Figure 7. Artificial repulsion with exponential repulsion function.

To prove the effectiveness, a comparison of the exponential repulsion function and repulsion function shown in equation (9) is made under slot condition. To ensure the vehicle will be tested by the slot, the start point is setted in the slot

$$U_{rep} = \begin{cases} 0.5K_{rep}\left(\frac{1}{d} - \frac{1}{d_0}\right)^2 (x - x_g)^2 & d \leq d_0 \\ 0 & d > d_0 \end{cases} \quad (9)$$

As shown in Figures 4–7, the artificial repulsion with exponential repulsion function is oscillating in a smaller scale while the amplitude of oscillation in contrastive example is hundreds of time larger. It shows the exponential repulsion function can prevent control signal saturation effectively.

The high-speed rotorcraft path planning based on the BBO algorithm

According to the original BBO introduced by Simon,[25] candidate solution is considered to be a vector of suitability index variable (SIV). A SIV vector is mapping a habitat suitability index (HSI), which represents the value of objective function mapped by candidate solution, of a species to a habitat. The species with high HSI is considered to have a large population and likely to emigrate. And species with low HIS is likely to accept immigration. The migration model is shown in equations (10) and (11)

$$\lambda_s = I(1 - f(k, n)) \quad (10)$$

$$\mu_s = Ef(k, n) \quad (11)$$

where λ_s is the immigration rate of the sth habitat and μ_s is the emigration rate of the sth habitat, I represents each island's maximum immigration rates, E represents the emigration rates, and k and n are the total number of species and the total population size, respectively. $f(k, n)$ represents the function of the total species number and the total population size.

In addition, a catastrophic ecological event can completely change the status of a habitat, which is known
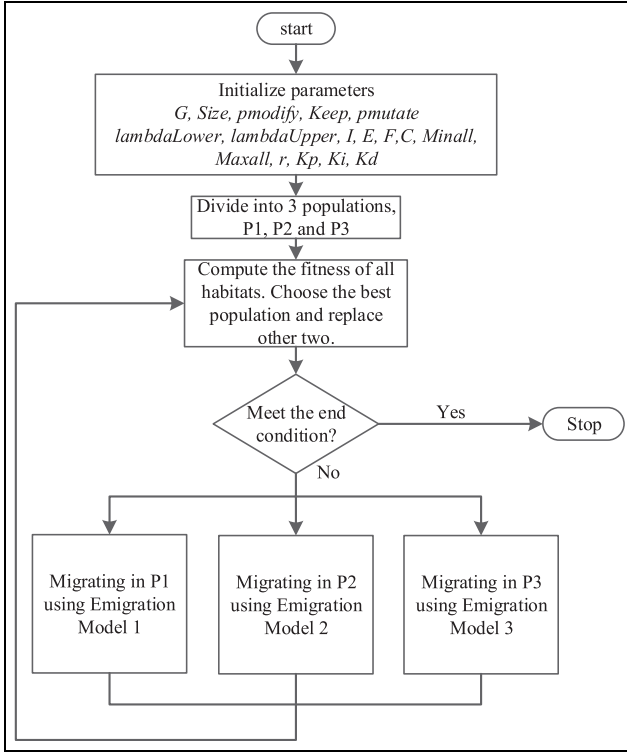
Figure 8. The flowchart of the EMM-BBO algorithm.

as a mutation when it is associated with BBO. It is known that the mutation probability function is inversely proportional to the number of habitats

$$m(x_i) = m_{max}\left(\frac{1 - P(s_i)}{P_{max}}\right) \qquad (12)$$

where m_{max} means the maximum value of mutation rate and P_{max} means the maximum number of habitats. The mutation function indicates that the habitat with the lowest HSI is most vulnerable to mutation, expanding and enriching the search target of the habitat.

To improve the performance of BBO, ensemble migration model is applied.[33] Sinusoidal model, square model, and linear model are used in different populations. The population which has the best habitat will replace other populations after each iteration.

According to BBO theory, the target function of path planning can be set to the fitness function of BBO. Limit the scale of velocity, acceleration, angular speed, and angular acceleration, select $k_{att}, k_{atv}, k_{rep}, l_{rep}, x_0$ as parameters to be adjusted.

Of the five selected parameters, k_{att} influences the magnitude of the artificial potential field, directly affects the speed of the high-speed rotorcraft flying toward the target position; k_{atv} is a parameter to ensure that the velocity of the high-speed rotorcraft is asymptotic stable near the target point, mainly used to control the speed of the high-speed rotorcraft near the target position; k_{rep} and l_{rep} influence the amplitude

and dynamic velocity of the repulsion curve; x_0 influences the displacement of the repulsion curve; these three parameters influence the effect of repulsive force.

The algorithm of path planning based on BBO is implemented as follows (Figure 8):

1. Initialize parameters where $Size = 45$ is the total population which is divided into three different parts for different migration models, $G = 30$ is the maximum generation, $pmodify = 1$ is the population migration probability, $Keep = 0$ is the population of elitists, $pmutate = 0.03$ is the probability of individual variation, $lambdaLower = 0$ and $lambdaUpper = 1$ is the boundary of immigration rate, $I = 1$ is the factor of immigration rate, $E = 1$ is the factor of emigration rate, $C = 1/30$ is the mutation probability, $Minall = [0.001, 0.1, 0.001, 0.001, 0]$ is the minimum value of the parameters to be adjusted $[k_{att}, k_{atv}, k_{rep}, l_{rep}, x_0]$, $Maxall = [0.5, 500, 0.1, 0.01, 20]$ is the maximum value of the parameters to be adjusted $[k_{att}, k_{atv}, k_{rep}, l_{rep}, x_0]$. Divided habitats into three populations
2. Compute the fitness value of all habitats (target function of path planning). Compare the different population, replace other populations with the best population. Reassign individuals with the same value to ensure that there are no identical individuals in the population.
3. Update populations. If the expected generation is reached, conclude the operation. Otherwise, continue the algorithm.
4. Carry out migration operation and variation operation in every habitats and go to step 2.

Mathematical simulation

Use a grid method to build an electronic map; set $200 \times 200 \times 100$ m planning space; design the typical obstacle combination, which a unit of space is $1 \times 1 \times 1$ m, and the grid space units with an obstacle are marked as 1, others are marked as 0, the high-speed rotorcraft looks for a path in the grid space flying to the target point. The simulation platform is MATLAB 2016a; the simulation computer's processor parameters are Intel(R)Core(TM)i5-7300HQ CPU at 2.5 GHz.

The simulation result under each condition is given as figures of flight path and flight characteristic curves.

Path planning under slot conditions

Set the starting point and destination, place multiple obstacles near the line between start point and destination point. The parameters of artificial potential field are selected by cut-and-trial method. The simulation conditions are set as shown in Table 1.
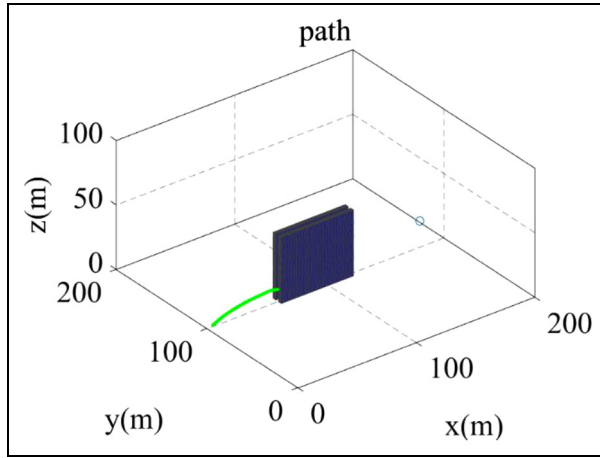
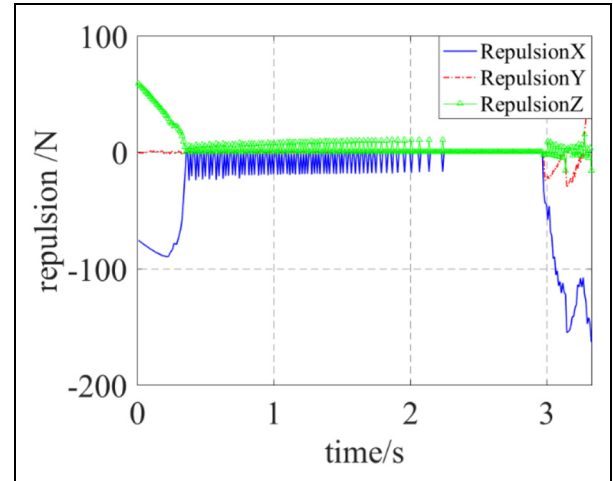**Figure 9.** Flight path under slot condition before BBO.

Table 1. Parameters under slot condition before BBO.

Parameters		
	Katt	0.07
	Krep	500
	Katv	0.08
	Lrep	0.003
	X0	12
Start point	[5, 100, 1]	
Initial track angle (°)	[0, 0]	
Target point	[180, 100, 20]	
Maximum acceleration (m/s^2)	50	
Maximum velocity (m/s)	20	
The action distance of repulsive force (m)	20	

BBO: biogeography-based optimization.
Simulation result: collision happens.

The parameters of repulsion function are setted by the method of trial and error.Figure 10 shows that the repulsive force is oscillating, which cause the heading angle changing dramatically. Therefore, the high-speed rotorcraft crashed into the wall.

The BBO optimization algorithm is used to carry out the path planning, simulated with the optimized potential field force parameters; the simulation conditions are set as shown in Table 2.

Figure 10 shows that before optimization, when high-speed rotorcraft fly into slot, the repulsive force varies dramatically, the amplitude is greater than 300 N and continues to increase. Figure 11 shows that the heading angle is increasing rapidly to 30°; at the same time, Figure 12 shows that high-speed rotorcraft fly at the speed of 20 m/s, the speed cannot be reduced in time. As shown in Figure 9, rotorcraft crashed into the wall in the end. Figures 13–15 illustrate that the optimized parameters decrease the repulsive force. When high-speed rotorcraft fly into the slot, the repulsion could keep stable, so the heading angle remains stable, the speed of rotorcraft decreases after entering the slit, smoothly through the slit (Figure 16).
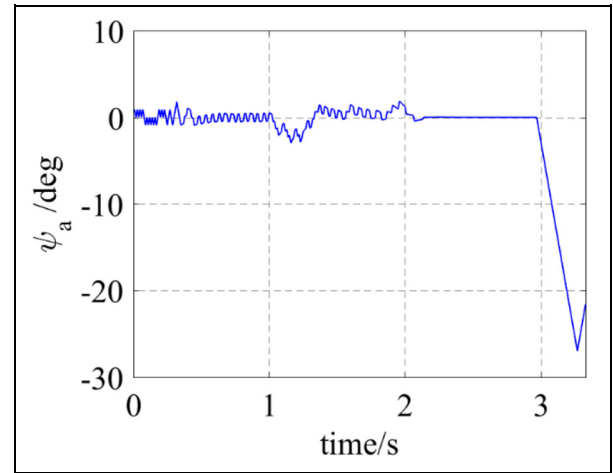

Figure 10. Repulsion under slot condition before BBO.

Figure 11. Heading angle under slot condition before BBO.

Table 2. Parameters under slot condition after BBO.

Parameters		
	Katt	0.314
	Krep	158.42
	Katv	0.088
	Lrep	0.0068
	X0	5.48
Start point	[5, 100, 1]	
Initial track angle (°)	[0, 0]	
Target point	[180, 100, 20]	
Max acceleration (m/s^2)	50	
Max velocity (m/s)	20	
The action distance of repulsive force (m)	20	

BBO: biogeography-based optimization.
Simulation result: flight time of 10.61 s, path length of 177.08 m, and average velocity of 16.69 m/s.

Path planning under multi-obstacle situation

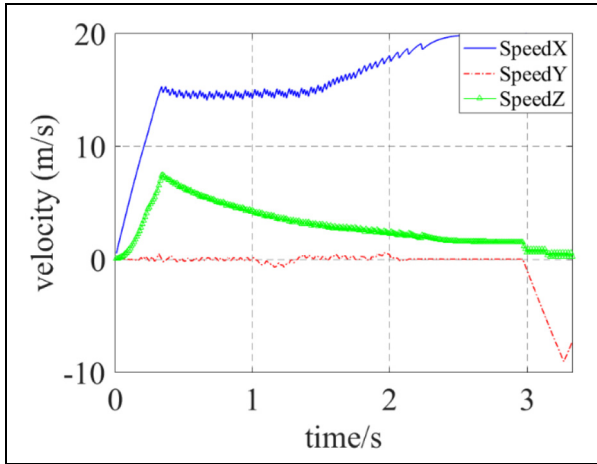Set the starting point and destination, place multiple obstacles near the line between start point and

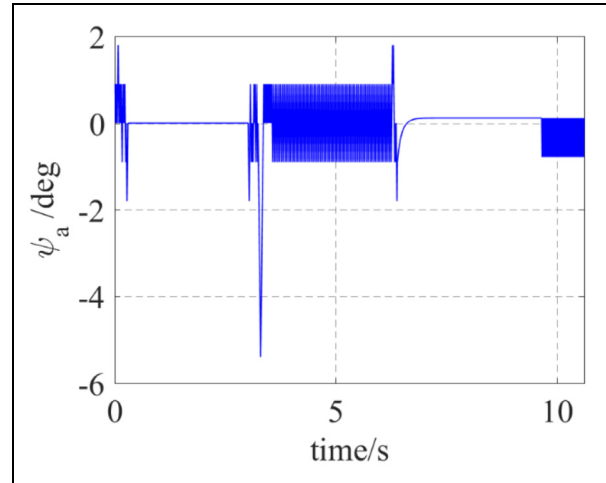**Figure 12.** Velocity under slot condition before BBO.

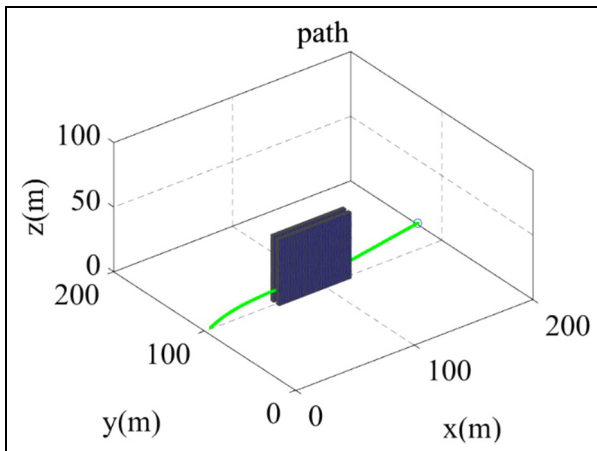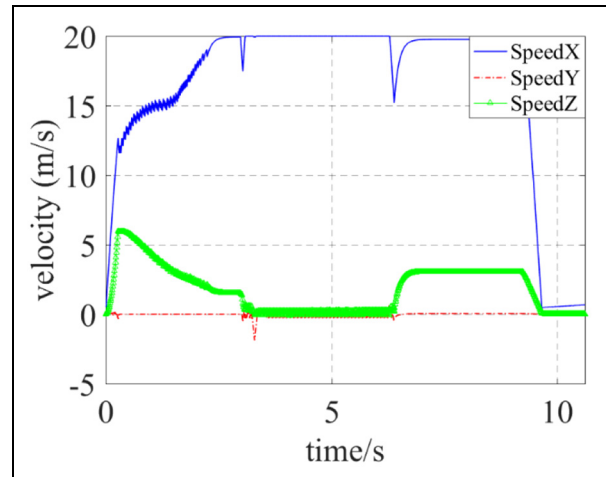**Figure 13.** Flight path under slot condition after BBO.
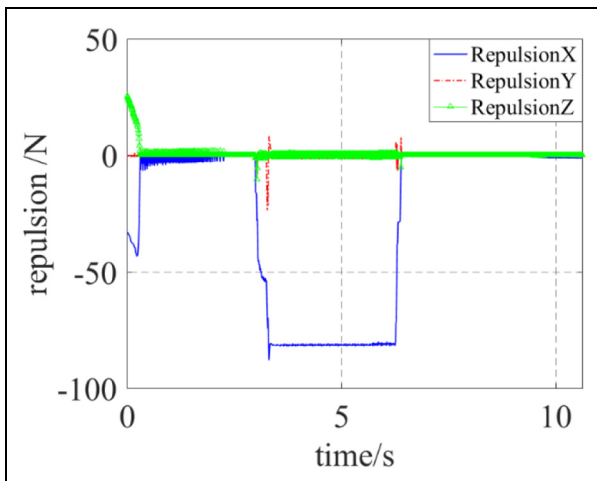

Figure 14. Repulsion under slot condition after BBO.

destination point. The parameters of artificial potential field are selected by cut-and-trial method. The

Figure 15. Heading angle under slot condition after BBO.

Figure 16. Velocity under slot condition after BBO.

simulation conditions are set as shown in Table 3. And the parameters of obstacles are set as shown in Table 4 in which (x, y, z) represents the position of the center of the rectangular obstacle and hx, hy, hz represent the half of border length of rectangular obstacle in x, y, z directions, respectively.

As shown in Figure 17, the path planning of artificial potential field method is realized by the potential field force parameter set based on trial and error method, the high-speed rotorcraft arrival the target point smoothly.

Next, the BBO optimization algorithm is used to carry out the path planning, simulated with the optimized potential field force parameters; the simulation conditions are set as shown in Table 5. And the parameters of obstacles are set as shown in Table 6 in which (x, y, z) represents the position of the center of the rectangular obstacle and hx, hy, hz represent the half of

**Table 3.** Parameters under multi-obstacles condition before BBO.

Parameters		
Parameters	*Katt*	0.07
	Krep	500
	Katv	0.08
	Lrep	0.003
	X0	12
Start point		[5, 5, 1]
Initial track angle (°)		[0, 0]
Target point		[170, 80, 30]
Maximum acceleration (m/s^2)		50
Maximum velocity (m/s)		20
The action distance of repulsive force (m)		20

BBO: biogeography-based optimization.

Table 5. Parameters under multi-obstacles condition after BBO.

Parameters		
Parameters	*Katt*	0.1777
	Krep	488.4178
	Katv	0.0599
	Lrep	0.0025
	X0	3.5918
Start point		[5, 5, 1]
Initial track angle (°)		[0, 0]
Target point		[170, 80, 30]
Max acceleration (m/s^2)		50
Max velocity (m/s)		20
The action distance of repulsive force (m)		20

BBO: biogeography-based optimization.

Table 4. Parameters of obstacles.

Number of obstacle	Position	1/2 length of side
1	$x = 100, y = 90, z = 11$	$hx = 1, hy = 30, hz = 10$
2	$x = 85, y = 95, z = 21$	$hx = 5, hy = 5, hz = 20$
3	$x = 50, y = 40, z = 11$	$hx = 5, hy = 5, hz = 10$
4	$x = 100, y = 35, z = 15$	$hx = 7, hy = 9, hz = 14$
5	$x = 120, y = 85, z = 31$	$hx = 5, hy = 12, hz = 30$
6	$x = 120, y = 50, z = 31$	$hx = 12, hy = 13, hz = 30$

Simulation result: flight time of 19.74 s, path length of 227.78 m, and average velocity of 11.54 m/s.

Table 6. Parameters of obstacles.

Number of obstacle	Position	1/2 Length of side
1	$x = 100, y = 90, z = 11$	$hx = 1, hy = 30, hz = 10$
2	$x = 85, y = 95, z = 21$	$hx = 5, hy = 5, hz = 20$
3	$x = 50, y = 40, z = 11$	$hx = 5, hy = 5, hz = 10$
4	$x = 100, y = 35, z = 15$	$hx = 7, hy = 9, hz = 14$
5	$x = 120, y = 85, z = 31$	$hx = 5, hy = 12, hz = 30$
6	$x = 120, y = 50, z = 31$	$hx = 12, hy = 13, hz = 30$

Simulation result: flight time of 11.17 s, path length of 192.6 m, and average velocity of 17.24 m/s.
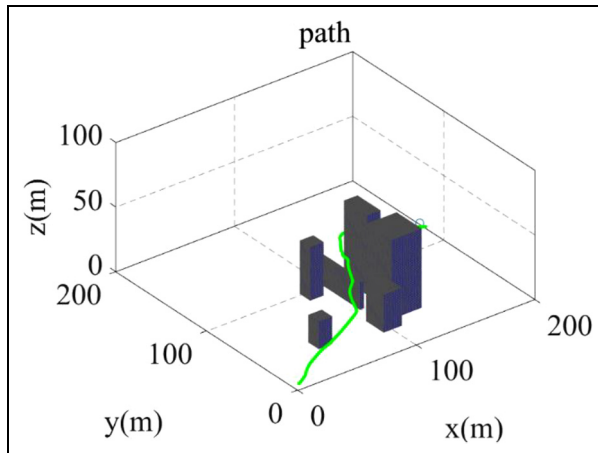
Figure 17. Flight path under multi-obstacles condition before BBO.

border length of rectangular obstacle in *x, y, z* directions, respectively.

Comparing the simulation result before and after optimization, as shown in Figure 17, a slit was formed between the two obstacles on the right, before the BBO optimization, the potential field force cannot control the high-speed rotorcraft flying through the slit, so the rotorcraft selects a longer way to go, and fly with a low speed. After BBO optimization, as shown in Figures 18–23, the scale of attractive force shrinks from −2~1.5 N to −0.6~1 N, the scale of repulsive force shrinks from −120~50 N to −170 N~50 N, the attractional action decreases and the repulsive force increases, this allows high-speed rotorcraft to bypass general obstacles and fly through the slit smoothly. Figures 20 and 24 show that the deceleration process is shortened and the reduction is smaller, the speed of flight is improved as result, besides, after BBO optimization, the frequency of acceleration and oscillation in the flight of a high-speed rotorcraft is greatly reduced, the path is smoother, the steering process is reduced, and energy are saved at the same time (Figure 25).

Conclusion

This article presents an artificial potential field path planning algorithm based on BBO optimization, to resolve the problem of high-speed rotorcraft path planning in three-dimensional space. The algorithm makes a quick operation to the problem of high dimension, complexity and limited calculation speed in three-dimensional path planning. Through simulation verification, the conclusion is obtained that the algorithm can effectively carry out the path planning of high-
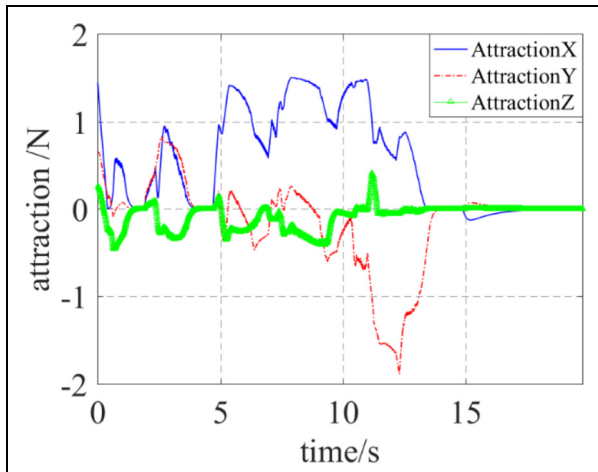
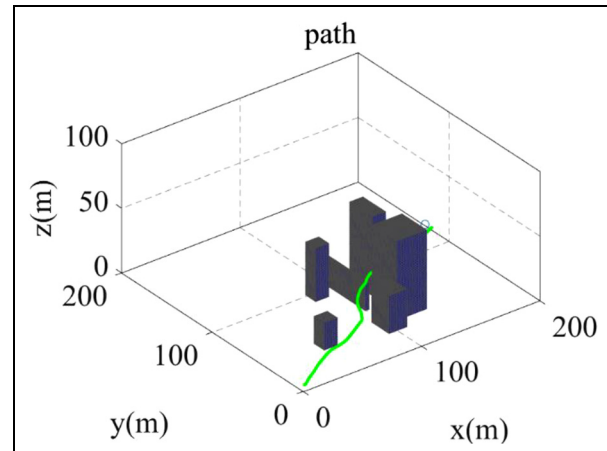**Figure 18.** Attraction under multi-obstacles condition before BBO.

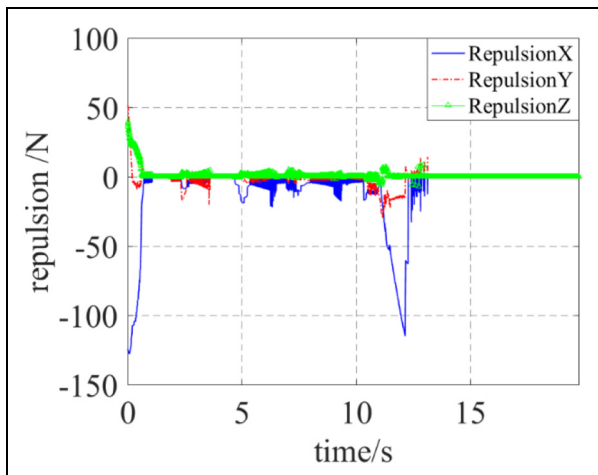**Figure 21.** Flight path under multi-obstacles condition after BBO.

Figure 19. Repulsion under multi-obstacles condition before BBO.
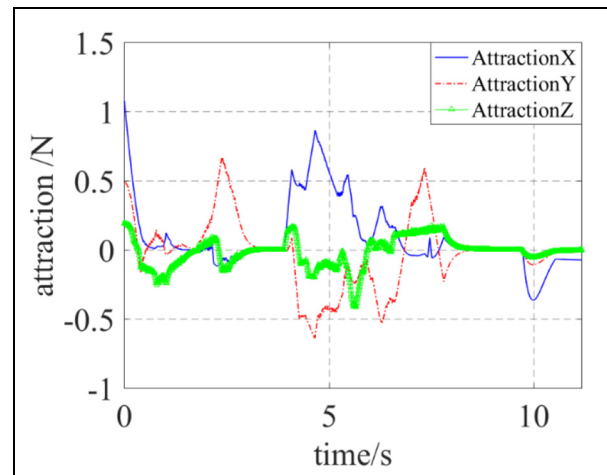

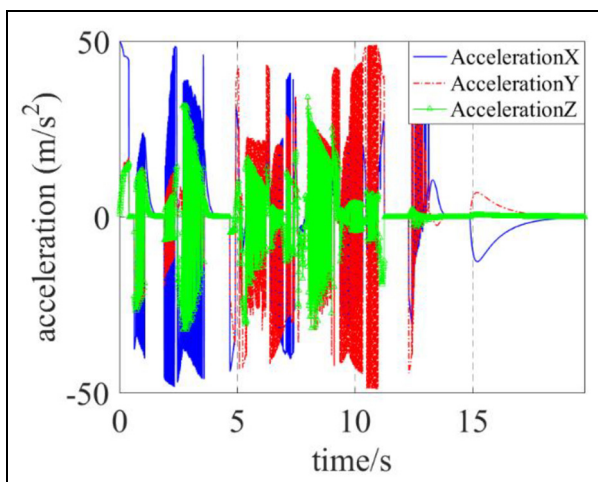**Figure 22.** Attraction under multi-obstacles condition after BBO.

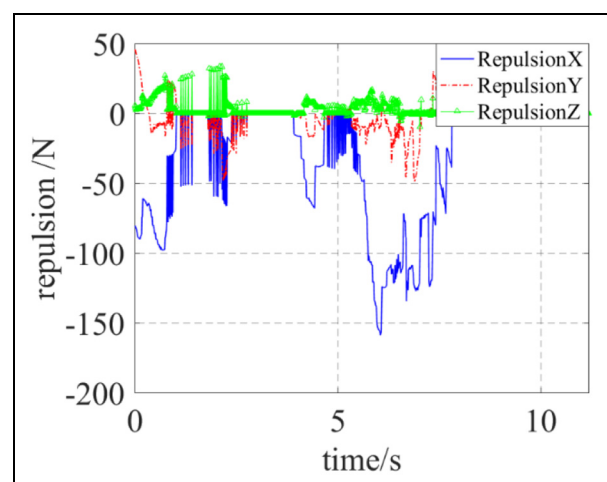**Figure 20.** Acceleration under multi-obstacles condition before BBO.

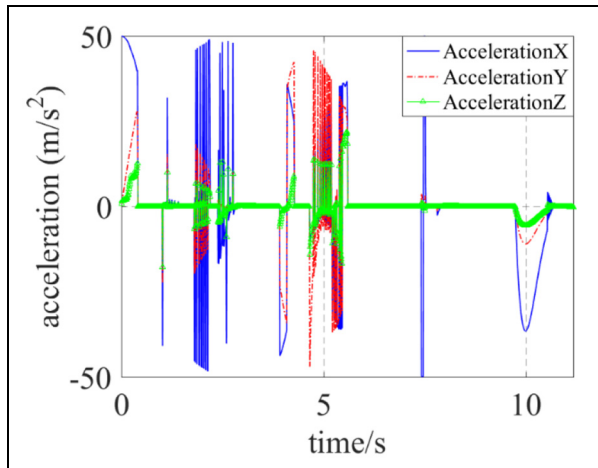**Figure 23.** Repulsion under multi-obstacles condition after BBO.

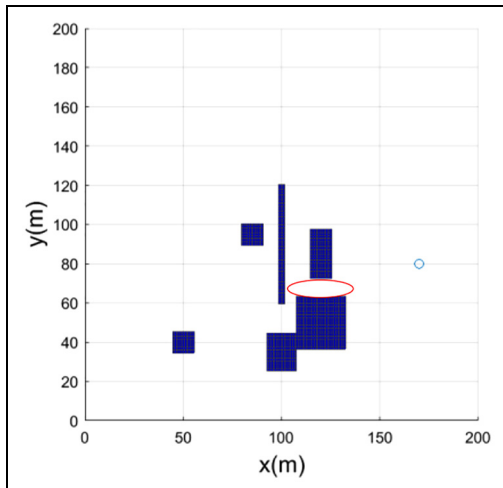**Figure 24.** Acceleration under multi-obstacles condition after BBO.

Figure 25. The diagram of obstacle split.

speed rotorcraft. The dynamic boundary of the aircraft was set up during the simulation, to ensure that the calculated path can be tracked by the rotorcraft. At the same time, a large number of simulation results prove the stability and reliability of the algorithm.

Acknowledgements

The authors thank the colleagues for their constructive suggestions and research assistance throughout this study. The authors also appreciate the associate editor and the reviewers for their valuable comments and suggestions.

Declaration of conflicting interests

The author(s) declared no potential conflicts of interest with respect to the research, authorship, and/or publication of this article.

ORCID iDs

Jia Song https://orcid.org/0000-0002-4019-970X
Mingfei Zhao https://orcid.org/0000-0002-6532-3471

References

1. Lupashin S and D'Andrea R. Adaptive fast open-loop maneuvers for quadrocopters. *Auton Robot* 2012; 33: 89–102.
2. Ritz R, Hehn M, Lupashin S, et al. Quadrocopter performance benchmarking using optimal control. In: *2011 IEEE/RSJ international conference on intelligent robots and systems (IROS)*, San Francisco, CA, 25–30 September 2011, pp.5179–5186. New York: IEEE.
3. Mellinger D, Michael N and Kumar V. Trajectory generation and control for precise aggressive maneuvers with quadrotors. *Int J Robot Res* 2012; 31: 664–674.
4. Yang C, Zhang D, Zhao X, et al. UAV 3D path planning based on IHDR autonomous-learning-framework. *Robot* 2012; 34: 513.
5. Bouktir Y, Haddad M and Chettibi T. Trajectory planning for a quadrotor helicopter. In: *IEEE 16th Mediterranean conference on control and automation*, Ajaccio, 25–27 June 2008, pp.1258–1263. New York: IEEE.
6. Duchoň F, Babinec A, Kajan M, et al. Path planning with modified a star algorithm for a mobile robot. *Procedia Engineer* 2014; 96: 59–69.
7. Wang H, Yu Y and Yuan Q. Application of Dijkstra algorithm in robot path-planning. In: *IEEE international conference on mechanic automation & control engineering*, Hohhot, China, 15–17 July 2011, pp.1067–1069. New York: IEEE.
8. Liu H, Stoll N, Junginger S, et al. A Floyd-Dijkstra hybrid application for mobile robot path planning in life science automation. In: *IEEE international conference on automation science and engineering*, Seoul, South Korea, 20–24 August 2012, pp.279–284. New York: IEEE.
9. Ferguson D and Stentz A. Using interpolation to improve path planning: the field D * algorithm. *J Field Robot* 2006; 23: 79–101.
10. Gemeinder M and Gerke M. GA-based path planning for mobile robot systems employing an active search algorithm. *Appl Soft Comput* 2003; 3: 149–158.
11. Masehian E and Sedighizadeh D. A multi-objective PSO-based algorithm for robot path planning. In: *IEEE international conference on industrial technology*, Vina del Mar, Chile, 14–17 March 2010, pp.465–470. New York: IEEE.
12. Khatib O. Real-time obstacle avoidance for manipulators and mobile robots. *Int J Robot Res* 1986; 5: 90–98.
13. Perez-Carabaza S, Besada-Portas E, Lopez-Orozco JA, et al. Ant colony optimization for multi-UAV minimum

time search in uncertain domains. *Appl Soft Comput* 2018; 62: 789–806.

14. Yao P, Xie Z and Ren P. Optimal UAV route planning for coverage search of stationary target in river. *IEEE T Contr Syst T* 2019; 27: 822–829.

15. Yin C, Xiao Z, Cao X, et al. Offline and online search: UAV multi-objective path planning under dynamic urban environment. *IEEE Internet Things* 2018; 5: 546–558.

16. Oral T and Polat F. MOD* Lite: an incremental path planning algorithm taking care of multiple objectives. *IEEE T Cybernetics* 2016; 46: 245–257.

17. Chen W, Wu X and Lu Y. An improved path planning method based on artificial potential field for a mobile robot. *Cybern Inform Tech* 2015; 15: 181–191.

18. Shi WR, Huang XH and Zhou W. Path planning of mobile robot based on improved artificial potential field. *J Comput Appl* 2010; 30: 2021–2023.

19. Ge SS and Cui YJ. New potential functions for mobile robot path planning. *IEEE T Robotic Autom* 2000; 16: 615–620.

20. Yu Z-Z, Yan JH, Zhao J, et al. Mobile robot path planning based on improved artificial potential field method. *J Harbin Inst Technol* 2011; 43: 349–354.

21. Wang SH, Zhao JF, Pan LF, et al. An evolutionary method of traditional artificial potential field. *Appl Mech Mater* 2012; 198–199: 1025–1029.

22. Zhang JY, Zhao ZP and Liu D. A path planning method for mobile robot based on artificial potential field. *J Harbin Inst Technol* 2006; 38: 1306–1309.

23. Kuang F and Wang YN. Robot path planning based on hybrid artificial potential field/genetic algorithm. *J Syst Simul* 2006; 18: 774–777.

24. Liu C. Anti-collision path planning for mobile robot based on modified potential field method. *J Southeast Univ* 2009; 39: 116–120.

25. Ergezer M, Dan S and Du D. Biogeography-based optimization. *IEEE T Evolut Comput* 2008; 12: 702–713.

26. Bhattacharya A and Chattopadhyay PK. Biogeography-based optimization for different economic load dispatch problems. *IEEE T Power Syst* 2010; 25: 1064–1077.

27. Sayed MM, Saad MS, Emara HM, et al. A novel method for tuning the PID parameters based on the modified biogeography-based optimization for hydraulic servo control system. In: *6th IET international conference on power electronics, machines and drives (PEMD 2012)*, Bristol, 27–29 March pp.1–5. Stevenage: The Institution of Engineering and Technology.

28. Luo D and Zhang HL. Hybrid biogeography-based optimization for solving tomato planting planning. *Agr Res* 2014; 3: 313–320.

29. Feng SL, Zhu QX, Zhong S, et al. Hybridizing adaptive biogeography-based optimization with differential evolution for global numerical optimization. *Appl Mech Mater* 2013; 457–458: 1283–1287.

30. Mi Z, Xu Y, Yu Y, et al. Hybrid biogeography based optimization for constrained numerical and engineering optimization. *Math Probl Eng* 2015; 2015: 423642.

31. Zheng YJ, Ling HF, Wu XB, et al. Localized biogeography-based optimization. *Soft Comput* 2014; 18: 2323–2334.

32. Zheng YJ, Ling HF and Xue JY. Ecogeography-based optimization: enhancing biogeogra-phy-based optimization with ecogeographic barriers and dif-ferentiations. *Comput Oper Res* 2014; 50: 115–127.

33. Ma H, Fei M, Ding Z, et al. Biogeography-based optimization with ensemble of migration models for global numerical optimization. In: *IEEE congress on evolutionary computation*, Brisbane, QLD, Australia, 10–15 June 2012. New York: IEEE.

34. Wang Y, Zhang MX and Zheng YJ. A hyper-heuristic method for UAV search planning. In: *International conference in swarm intelligence*, Fukuoka, Japan, 27 July–1 August 2017. Cham: Springer.

35. Mahony R, Kumar V and Corke P. Multirotor aerial vehicles: modeling, estimation, and control of quadrotor. *IEEE Robot Autom Mag* 2012; 19: 20–32.